DECLASSIFIED [redacted] Copy 61 72403

NASA TM X-579

NASA TM X-579

[redacted]

[redacted]

TECHNICAL MEMORANDUM

X-579

Declassified by authority of NASA
Classification Change Notices No. 115
Dated **6/21/62

EFFECTIVENESS OF SEVERAL CONTROL ARRANGEMENTS

ON A MERCURY-TYPE CAPSULE

By Robert I. Sammonds and Robert R. Dickey

Ames Research Center
Moffett Field, Calif.

[redacted]

[redacted]

[redacted]

NATIONAL AERONAUTICS AND SPACE ADMINISTRATION

WASHINGTON [redacted] October 1961

[redacted]

1Z

NATIONAL AERONAUTICS AND SPACE ADMINISTRATION

TECHNICAL MEMORANDUM X-579

EFFECTIVENESS OF SEVERAL CONTROL ARRANGEMENTS ON A MERCURY-TYPE CAPSULE*

By Robert I. Sammonds and Robert R. Dickey

SUMMARY

An investigation has been conducted to determine the trim effectiveness of three types of aerodynamic controls (flaps) on a Mercury-type capsule and their effect on the static and dynamic stability of the model. The flap types investigated consisted of (1) an outward extension of the spherical surface of the front face beyond the surface of the cone (spherical flap), (2) a forward extension of the conical surface of the afterbody ahead of the spherical front face (conical flap), and (3) a flat surface perpendicular to the longitudinal axis of the capsule at the juncture of the spherical front face and the conical afterbody (flat flap). Tests were made in a wind tunnel at a Mach number of 3.3 and a Reynolds number of 1.25, based on the maximum diameter of the capsule, and in free flight at a Mach number of 5.5 and a Reynolds number of 0.1 million.

Results of these investigations showed that the conical-type flap had the greatest effectiveness. A flap area equal to approximately 6-1/2 percent of the capsule frontal area would trim the capsule at an angle of attack of -29°, resulting in a lift-drag ratio of approximately 0.45. The spherical flap was the least effective, contributing a moment increment only one-third as great as the conical flap.

The addition of the flaps to the basic model increased the drag but did not appreciably affect either the lift-drag ratio, lift-curve slope, or the static stability. For all the configurations tested, the capsule had a negative lift-curve slope and was statically stable. The model generally remained dynamically unstable with the addition of flaps; however, with certain sizes of the conical flap the model was dynamically stable.

*Title, Unclassified

INTRODUCTION

The use of lift on a vehicle entering the earth's atmosphere from space-flight missions increases the depth of the permissible entry corridor and also permits the vehicle to maneuver in the atmosphere toward a desired landing point. Trajectory analyses (e.g., refs. 1 and 2) indicate that only a modest lift-drag ratio is necessary to produce beneficial effects. Capsule configurations, such as the Mercury capsule, for example, can generate high enough lift-drag ratios to realize a substantial gain in the entry corridor depth and a useful degree of control over landing point.

Capsule configurations can, in principle, be trimmed at lifting attitudes by offsetting the center of gravity or by the use of reaction or aerodynamic controls. In reference 3, the use of center-of-gravity offset was investigated as a means of trimming a Mercury-type capsule to the desired attitudes. In the present report, a study is presented of aerodynamic controls (flaps attached to the corner of the front face) for the same configuration.

A
5
0
0

The model investigated had a spherical segment front face, with a radius equal to the frontal diameter, and a conical afterbody of 26.5° half angle. This afterbody was chosen so that at the lifting attitudes of interest, the afterbody would not be exposed to large pressure forces or large heating rates. Several different flap geometries were investigated.

The tests were conducted in the Ames 1- by 3-Foot Supersonic Wind Tunnel No. 1 at a Mach number of 3.3, and in the Ames Pressurized Ballistic Range at a Mach number of 5.5. The Reynolds numbers, based on the maximum face diameter, were 1.25 and 0.1 million, respectively. The results obtained are compared with available simple theories to see if flap effectiveness is predictable.

NOTATION

General

A_f area of flap, sq ft

C_D drag coefficient, $\frac{\text{drag}}{q_\infty S}$

C_p pressure coefficient, $\frac{p_l - p_\infty}{q_\infty}$

d	reference diameter (diameter of front face), ft
l	length of flap extension, ft
M	free-stream Mach number
p	static pressure, lb/sq ft
q	dynamic pressure, lb/sq ft
R	radius of curvature of spherical front face, ft
S	reference area, $\frac{\pi d^2}{4}$, sq ft
x, y, z	earth-fixed system of axis; also displacements along these axes, ft
α_{trim}	angle of attack for $C_m = 0$, deg
δ	angle between the tangent to the local surface of the body and the free-stream direction, deg
θ	angle subtended by the edges of the flap in a plane normal to the longitudinal axis of the capsule, deg
ρ	air density, slugs/cu ft
Ω	cone half angle, deg

A
5
0
0

Wind Tunnel

C_L	lift coefficient, $\frac{\text{lift}}{q_\infty S}$
C_m	pitching-moment coefficient, $\frac{\text{pitching moment}}{q_\infty Sd}$
$\frac{L}{D}$	lift-drag ratio
α	angle of attack (angle between the longitudinal axis of the capsule and the free-stream direction), deg

Free Flight

C_{L_α} lift-curve slope, per radian

C_{m_α} restoring-moment-curve slope (equivalent to pitching-moment-curve slope used in the wind tunnel), $-\dfrac{8\pi^2 I_y}{\lambda^2 \rho S d}$, per radian

$C_{m_q} + C_{m_{\dot{\alpha}}}$ damping-in-pitch derivative, sec^{-1}

I_y average transverse moment of inertia, slug-ft^2

α angle of attack (angle between the longitudinal axis of the capsule and the free-stream direction projected onto the x, z plane), deg

α_r resultant angle of attack, $\sqrt{\alpha^2 + \beta^2}$, deg

α_{RMS} root-mean-square resultant angle of attack, $\sqrt{\dfrac{\int_0^x \alpha_r^2 dx}{x}}$, deg

β angle of sideslip (angle between longitudinal axis of the capsule and the free-stream direction projected onto the x, y plane), deg

λ wave length of pitching oscillation with respect to the air stream, $\dfrac{2\pi}{\sqrt{\omega_1 \omega_2}}$, ft

ξ dynamic stability parameter, $C_D - C_{L_\alpha} + (C_{m_q} + C_{m_{\dot{\alpha}}}) \left(\dfrac{d}{\sigma}\right)^2$

σ transverse radius of gyration, $\dfrac{I_y}{d^2}$, ft

ω_1, ω_2 rates of rotation of complex vectors which generate the model pitching motion (see ref. 6), radians/ft

$(\dot{\ })$ first derivative with respect to time

Subscripts

∞ free-stream condition

l local condition after bow shock

MODELS

The basic configuration tested was a body of revolution consisting of a 26.5° half-angle conical afterbody and a spherical segment front face, having a face diameter to radius-of-curvature ratio (d/R) equal to 1. The cone half angle of 26.5° was selected in accordance with the considerations presented in the Introduction and in reference 3.

Three types of aerodynamic controls, shown in the sketches of figure 1, were investigated in conjunction with the basic model: (1) an outward extension of the spherical surface beyond the cone, (2) a forward extension of the conical surface ahead of the spherical front face, and (3) a flat surface perpendicular to the longitudinal axis of the capsule at the juncture of the spherical front face and the conical afterbody. These three flap configurations are hereinafter referred to as the "spherical," "conical," and "flat" flaps, respectively. As shown in figure 1(a), the wind-tunnel models consisted of three different sized spherical flaps and one each of the conical- and flat-type flaps. The free-flight models, as shown in figure 1(b), consisted of four different sized spherical flaps and four different sized conical flaps. Photographs of the flap installation on the wind-tunnel and free-flight models are shown in figures 2 and 3, respectively. The variation of the flap area with θ and l is presented in figure 4.

The wind-tunnel models had a portion of their afterbodies removed to facilitate mounting them on the tunnel support system. The models tested in free flight were of homogeneous construction, having their centers of gravity located at 0.33 of the maximum diameter aft of the front face. This location was taken to be the moment center for all of the free-flight and wind-tunnel tests.

TESTS AND REDUCTION OF DATA

The procedures used and the accuracies obtained for each facility will be briefly described.

Wind-Tunnel Tests

The lift, drag, and pitching moment of the models were measured at angles of attack from $+30^\circ$ to -45° by means of a flexure-type strain-gage balance. The balance extended rearward from the base of the model and was shielded from the air stream by a 7/8-inch-diameter shroud.

The effects of wall interference, tunnel stream angle, and pressure gradients are believed to be negligible for these tests. The base drag correction arising from the difference between the free-stream static pressure and the static pressure measured at the cut-off base of the model was found to be small and is not included in the coefficients presented in this report.

A
5
0
0

The mean square values of the random errors of measurement, evaluated by the method of reference 4, are given in the following table:

M	± 0.02
α	$\pm 0.10^\circ$
C_L	± 0.010
C_D	± 0.016
C_m	± 0.012
L/D	± 0.010

Pressurized-Ballistic-Range Tests

Models were launched in free flight from a caliber 50 powder gas gun at initial muzzle velocities of approximately 6300 feet per second. The models were adapted to the gun by means of a two-piece plastic (Lexan) sabot which launched the model at nearly its design trim angle. Photographs of two of the flapped models and their 20° canted sabots are shown in figure 3.

Shadowgraph pictures, triggered by the model, were obtained in 2 orthogonal planes at 17 observation stations, for a ballistic flight of 130 feet. The photographic observation stations are calibrated and referenced in such a manner that the spatial position and the attitude of the model at each station may be determined with respect to an orthogonal system of axes for the entire range. An electronic chronograph was used to measure the time of flight between stations. The accuracies involved in determining the model position, orientation, and time of flight are as follows:

x, y, z	± 0.005 inch
α, β	$\pm 0.1^\circ$

The reduction of the trajectory data to force and moment coefficients was accomplished by the method described in reference 5. By this method the best suited aerodynamic coefficients and initial conditions are selected by an iterative process to fit the equations of motion to the particular motion under consideration. In the present case, the equations of motion given in reference 6 were used to obtain the stability coefficients and lift-curve slope (including the effects of trim and roll). For the flapped models of this investigation, the reduction of the trajectory data to force and moment coefficients on the basis of these formulas is complicated by the fact that the models are not axially symmetric and were trimmed to fly at angle of attack. However, it has been shown in reference 6 that the equations of motion are applicable to models with small amounts of asymmetry and relatively low amplitudes of oscillation and that they can be solved for both roll rate and trim angle. The degree to which the iterative process converges in fitting these equations of motion to the experimental data is indicative of the accuracy with which the experimental data can be matched. Motions having large oscillation amplitudes (greater than about $\pm 20^{\circ}$) and/or large trim angles (greater asymmetry) either did not converge at all or did not converge to a reasonable degree of accuracy so that is was not possible to analyze these runs by the above method. However, the trim angle of attack can be determined from the positions of the tricyclic vectors (ref. 6) on a plot of α versus β.

A
5
0
0

In addition, runs in which the model has negligible roll and does not precess (see ref. 6) can be analyzed to determine trim angle and static stability by fitting the motions of the model to sine waves. This method of analysis, like the more general method of reference 6, assumes that the model has linear aerodynamic moment coefficients. For the data presented herein, the machine fit to α and β resulted in RMS errors of less than $\pm 1.5^{\circ}$ for all cases except that the error was $\pm 2.5^{\circ}$ with the 90° conical flap ($\alpha_{trim} = -15^{\circ}$).

The drag coefficients presented herein for the free-flight models were reduced basically by the method of reference 7, which was modified to allow for variations of the drag coefficient with angle of attack.

A procedure applicable to cases where the drag coefficient varies with the angle of attack squared is presented in reference 8. For the present investigation, the assumed variation of drag coefficient with resultant angle of attack was modified by the addition of a fourth-power term as described in reference 3. However, it can still be shown, in a manner similar to that used in reference 8, that the effective constant drag coefficient obtained from the present data by the method of reference 7, and under the same constraints, is equivalent to the drag coefficient that would be obtained at a constant angular displacement equal to the root-mean-square angle of attack, averaged over the distance interval of the trajectory.

RESULTS AND DISCUSSION

Wind-Tunnel Tests

Force and moment data obtained from the wind-tunnel tests are presented in figures 5 through 8 as a function of angle of attack.

Basic capsule.- Figure 5 shows a comparison of the measured values of C_L, C_D, C_m, and L/D for the basic capsule with those predicted by modified Newtonian impact theory ($C_p = 1.76 \sin^2\delta$). Two theoretical curves are presented for angles of attack greater than 26-1/2° - one based on the front face alone and the other including the effect of the afterbody. In general, agreement between theory and experiment is quite good, especially at angles of attack up to ±25°. Above 25°, better agreement between theory and experiment is obtained where the effect of the afterbody is included in the theory. It can be noted that the capsule develops lift-drag ratios above 0.5 in the angle range above 35°, at lift coefficients between 0.4 and 0.5; C_{m_α} becomes rather small and possibly negative above 40° angle of attack.

Capsule with the three basic types of flap controls.- Figure 6 presents a comparison of the measured values of C_L, C_D, C_m, and L/D for the basic capsule and for the three different flapped configurations (spherical, conical, and flat) having equivalent sized flaps ($l/d = 0.09$, $\theta = 45°$, $A_f/S = 0.049$). For all flap types, the capsule was statically stable at trim attitude. The conical type was the most effective for a given flap area; that is, it trimmed the capsule ($C_m = 0$) at the highest negative angle of attack and thus developed the highest trimmed lift-drag ratio, 0.42 at trim. The nearly linear variation of the lift-drag ratio with angle of attack obtained for these configurations indicates that trim angles in excess of 30° will be required to produce lift-drag ratios of the order of 0.5 for this face curvature. (See ref. 3 for a discussion of the effect of face curvature on L/D.)

Figure 7 presents a comparison of the measured values of C_L, C_D, C_m, and L/D for three different sized spherical flaps ($A_f/S = 0.049$, 0.067, 0.098).

ΔC_m.- Incremental values of pitching-moment coefficient for the three types of flaps, obtained by subtracting the pitching moment of the basic model from the total pitching moment of the model with flaps, are presented in figure 8. These data clearly show the superiority of the conical flap at the higher negative angles of attack. Incremental pitching moments predicted for the flaps by modified Newtonian impact theory, shown by the dashed lines, are in error for the conical flaps because a stagnation point in the flow can be expected to occur on the windward surface of these flaps. Although it is not entirely logical to assume that the stagnation pressure occurs over the entire windward

surface of the flap because of end effects, etc., this assumption appears to give a good first approximation for predicting the effect of the flap. On this basis, equation (A1) was used to predict incremental values of pitching moment due to the flap. The predicted values of ΔC_m, presented in figure 8, show better agreement with the experimental results than those predicted by impact theory, although this method still underestimates the flap effectiveness at negative angles of attack. At high negative angles of attack ($\alpha < -20^\circ$ for these test conditions), a secondary shock associated with the flap reduces the flap effectiveness; equations (A2) were used to predict incremental values of pitching moment and reasonable agreement was obtained with the experimental data.

A
5
0
0

Free-Flight Tests

Force, trim, and static and dynamic stability data derived from free-flight tests of the basic model (ref. 3) and of two of the flapped configurations (spherical and conical) are presented in figures 9 through 13.

Trim effectiveness.- The data presented in figure 9 show the trim effectiveness of various sized flaps of both the spherical and conical types. These data show that the flap effectiveness is directly a function of the flap area and type and is not particularly a function of either θ or l, except insofar as they are effective in changing the flap area. A conical-type flap having an area ratio (A_f/S) of 0.06 would trim the capsule at approximately 26-1/2°, which is better than three times as effective as a spherical flap of comparable size.

In the case of the spherical flap, figure 9(a), it can be seen that the experimental data obtained in free flight agree well with that predicted by modified Newtonian impact theory ($C_{p_t} = 1.8$, appropriate to the test Mach number). Included in figure 9(a) are experimental values of α_{trim} obtained from the wind-tunnel tests (fig. 7). These data agree within the experimental uncertainty (indicated by horizontal length of the bars) with impact theory and with the free-flight results.

In the case of the conical flap, figure 9(b), agreement of the experimental data with impact theory is poor, as noted earlier. However, theoretical values of trim angle of attack, predicted by equations (A1) and (A2) of the appendix, show reasonable correlation with the free-flight data. Comparison of the free-flight data with that obtained in the wind tunnel shows that the wind-tunnel test gave a considerably higher trim angle of attack. It is felt that this lack of agreement is due to afterbody effects resulting from the fact that the wind-tunnel models had a portion of their afterbodies removed to accommodate the model support system.

Drag.- Drag coefficients presented in figure 10 show that, in spite of the differences in Mach number and Reynolds number, good agreement between free-flight and wind-tunnel results was obtained for the basic configuration and for models with comparable sized spherical- and conical-type flaps. Comparison of the experimental data for the basic configuration with modified impact theory also shows good agreement, especially at the high angles of attack.

It should be pointed out that the angles of attack presented for the free-flight data have been determined from a root mean square of the resultant angle of attack, as described in the section on Reduction of Data, and are equivalent to the angles of attack obtained in the wind tunnel.

Lift.- Lift-curve slopes presented in figure 11 for the free-flight models, as a function of α_{RMS}, show very little effect of either flap size or shape. Comparison of these data with the wind-tunnel data or with theory is not possible because these lift-curve slopes are averages for an oscillating model. However, these data show a decrease in lift-curve slope with increasing angle of attack. This decrease is indicative of a nonlinear variation in lift with angle of attack similar to that obtained in the wind-tunnel tests (figs. 5 and 7). Ticks have been included on the figure to show the lift-curve slope predicted by Newtonian theory for the basic model at 0° angle of attack.

Stability.- The effect of the spherical- and conical-type flaps on the static and dynamic stability of the basic model can be seen in figures 12 and 13. The data presented in figure 12 show that the capsule remained statically stable with either type of flap. It should be noted that these data are average values and depend on the magnitude of the oscillation of the capsule, and that they have been plotted versus α_{RMS} for convenience only.

Comparison of the dynamic stability data for these two flap configurations and for the basic model (fig. 13) shows that the addition of the 45° conical flap to the basic model made the model dynamically stable. Adding the spherical, or the 90° conical flap to the basic model, however, generally had no appreciable effect on the dynamic stability. A model with four conical flaps ($\theta = 45^{\circ}$) symmetrically located at 90° intervals was tested to determine whether two flaps in each orthogonal plane would make the capsule more stable than a single flap. The results of this experiment (one test shot) show that an increase in the number of flaps from one to four also caused a decrease in stability. It should be pointed out that a value of damping parameter (ξ) of +2 is equivalent to about a 5 percent divergence in amplitude per cycle of oscillation at the conditions of the test.

<u>Flow and shock-wave patterns</u>.- The shadowgraph pictures presented in figures 14 and 15 give some insight into the observed aerodynamic behavior of the flaps in terms of their flow configurations. A brief discussion of some of the more interesting features follows.

At high positive angles of attack (30°) the conically flapped model has a more closely wrapped bow wave on the windward side than either of the other two configurations. At 30° angle of attack there is evidence of flow separation off the spherical and flat-type flaps but none from the conical flap. It should be pointed out that the bottom surfaces of the cone and the flap are exposed to the air stream (windward surfaces) which tends to encourage attached flow at the corner on the conical flap. At high negative angles of attack (-45°), both the conical and flat-type flap configurations have compression waves associated with the flaps and separated regions on the front face. Photographs taken at lower angles of attack, but not presented herein, show that the shock wave associated with the flat-type flap persists to a smaller angle of attack than that for the conical flap, although the conical flap model appears to have considerably more separated flow over the front face. The spherical flap model, on the other hand, had no apparent separated region on the front face. For all of the wind-tunnel models, at high negative angles of attack, reattachment shock waves on the windward surface of the conical afterbody just behind the corner of the front face are indicative of a local separation bubble at the corner.

It can be seen that the observed flow conditions at negative angle of attack correlate well with the flow patterns assumed in the analysis given in the appendix and that, as would be expected from the theory, the most effective configuration is that having the strongest flap shock wave and/or the largest region of separated flow on the face of the model.

Shadowgraph pictures from the free-flight tests, figure 15, show substantially the same characteristics as noted from the wind-tunnel pictures, except that, due to the higher Mach number, the shock wave standoff distance is smaller.

CONCLUSIONS

Data have been presented herein showing the trim effectiveness of several types of aerodynamic controls (flaps) on a Mercury-type capsule and their effect on the static and dynamic stability of the capsule. These data, obtained from tests in a wind tunnel at a Mach number of 3.3 and a Reynolds number of 1.25 million (based on the maximum face diameter) and in free flight at a Mach number of 5.5 and a Reynolds number of 0.1 million, indicate the following:

1. The trim effectiveness of the conical flap was superior to that of the flat and spherical types, resulting in a trim angle of attack of approximately -29° for a flap size equal to 6.3 percent of the capsule frontal area. For the spherical flap, however, the same size flap resulted in a trim angle of attack of only -9°.

2. For a given angle of attack, the effect of the size and shape of the flap on the lift-drag ratio was small. Extrapolation of these data shows that at trim angles of attack, around 35°, lift-drag ratios of the order of 0.5 are obtained.

3. The static stability of the basic configuration was not greatly affected by the addition of flaps. However, the conical-type flaps were slightly destabilizing, whereas the spherical type were slightly stabilizing. In all cases, the capsule was statically stable at the trim angle of attack.

A
5
0
0

4. The dynamic stability of the basic configuration was increased by the addition of the 45° conical flap but was relatively unaffected by either the spherical or 90° conical flaps. In all cases, the 45° conically flapped models were dynamically stable, whereas the spherically and 90° conically flapped models were generally dynamically unstable.

5. Modified Newtonian impact theory predicted quite well the effectiveness of the spherical flap and reasonably well the effectiveness of flat-type flaps, but badly underestimated the effectiveness of the conical flap. However, on the assumption that stagnation pressure acts on the flap face, it is possible to predict the characteristics of the conical flap.

Ames Research Center
National Aeronautics and Space Administration
Moffett Field, Calif., Aug. 11, 1961

APPENDIX A

FORMULAS FOR PREDICTING THE FLAP EFFECTIVENESS OF THE CONICAL-TYPE FLAP

If the windward side of the flap is assumed to be at stagnation pressure, the effectiveness of the conical-type flap is

A500

$$\Delta C_{m_f} = -\frac{2C_{p_t}}{SR}\int_0^{\theta/2}\int_{r_1}^{r_2}\left[\frac{r^2\cos\theta}{\sin^2\Omega} - \frac{\bar{C}}{\tan\Omega}(r\cos\theta)\right] dr\, d\theta \qquad \text{(A1)}$$

where

C_{p_t} = total pressure coefficient across a normal shock

$r_1 = d/2$

r_2 = the radial distance from the longitudinal center line of the model to the leading edge of the flap, $r_1 + l \sin\Omega$

$$\bar{C} = R\left[\frac{1}{2\tan\Omega} + (1 + \Delta) - \frac{\sqrt{R^2 - r_1^2}}{R}\right]$$

Δ = center-of-gravity location, in percent of the maximum face diameter, aft of the front face

However, as the angle of attack becomes more negative, a point will be reached at which the local flow over the front face of the model will become supersonic, resulting in a secondary shock wave associated with the flap. When this condition occurs $(M_1 \geq 1.0)$, the pressures on the flap can be calculated by means of the embedded Newtonian flow theory of reference 9, specifically by use of the equation

$$C_{p_f} = C_{p_l} + 2\left(\frac{q_1}{q_\infty}\right)\sin^2\mu = C_{p_t}\sin^2\delta + 2\left(\frac{q_1}{q_\infty}\right)\sin^2\mu$$

where μ is the angle between the secondary shock and the surface of the model. For the data presented herein, the secondary shock was assumed to be a normal shock ($\mu = 90^\circ$).

Thus, for these conditions ($M_1 \geq 1.0$, as determined by Newtonian concepts) the equation for the flap effectiveness can be given by

$$\Delta C_{m_f} = -\frac{2C_{p_f}}{SR}\int_0^{\theta/2}\int_{r_1}^{r_2}\left[\frac{r^2\cos\theta}{\sin^2\Omega} - \frac{\bar{C}}{\tan\Omega}(r\cos\theta)\right]dr\,d\theta \qquad \text{(A2)}$$

It is expected that the above equations will tend to underestimate the effectiveness of the flaps because interference of the flap with flow on the model front face has not been accounted for. This interference will produce local regions of increased pressure on the model face and contribute to the total pitching-moment increment attributable to deflection of the flap.

A
5
0
0

REFERENCES

1. Chapman, Dean R.: An Analysis of the Corridor and Guidance Requirements for Supercircular Entry Into Planetary Atmospheres. NASA TR R-55, 1959.

2. Levy, Lionel L., Jr.: An Approximate Analytical Method for Studying Atmosphere Entry of Vehicles With Modulated Aerodynamic Forces. NASA TN D-319, 1960.

3. Intrieri, Peter F.: Effects of Transverse Center-of-Gravity Displacement, Afterbody Geometry, and Front-Face Curvature on the Aerodynamic Characteristics of Mercury-Type Models at a Mach Number of 5.5 NASA TM X-569, 1961.

4. Beers, Yardley: Introduction to the Theory of Error. Addison-Wesley Publishing Co., Cambridge, Mass., 1953.

5. Sommer, Simon C., Short, Barbara J., and Compton, Dale L.: Free-Flight Measurements of Static and Dynamic Stability of Models of the Project Mercury Re-entry Capsule at Mach Numbers 3 and 9.5. NASA TM X-373, 1960.

6. Nicolaides, John D.: On the Free Flight Motion of Missiles Having Slight Configurational Asymmetries. BRL Rep. 858, Aberdeen Proving Ground, 1953 (IAS Preprint 395).

7. Seiff, Alvin: A New Method for Computing Drag Coefficients From Ballistic Range Data. Jour. Aero. Sci., vol. 25, no. 2, Feb. 1958, pp. 133-134.

8. Seiff, Alvin, and Wilkins, Max E.: Experimental Investigation of a Hypersonic Glider Configuration at a Mach Number of 6 and at Full-Scale Reynolds Numbers. NASA TN D-341, 1961.

9. Seiff, Alvin, and Whiting, Ellis E.: The Effect of the Bow Shock Wave on the Stability of Blunt-Nosed Slender Bodies. NASA TM X-377, 1960.

A
5
0
0

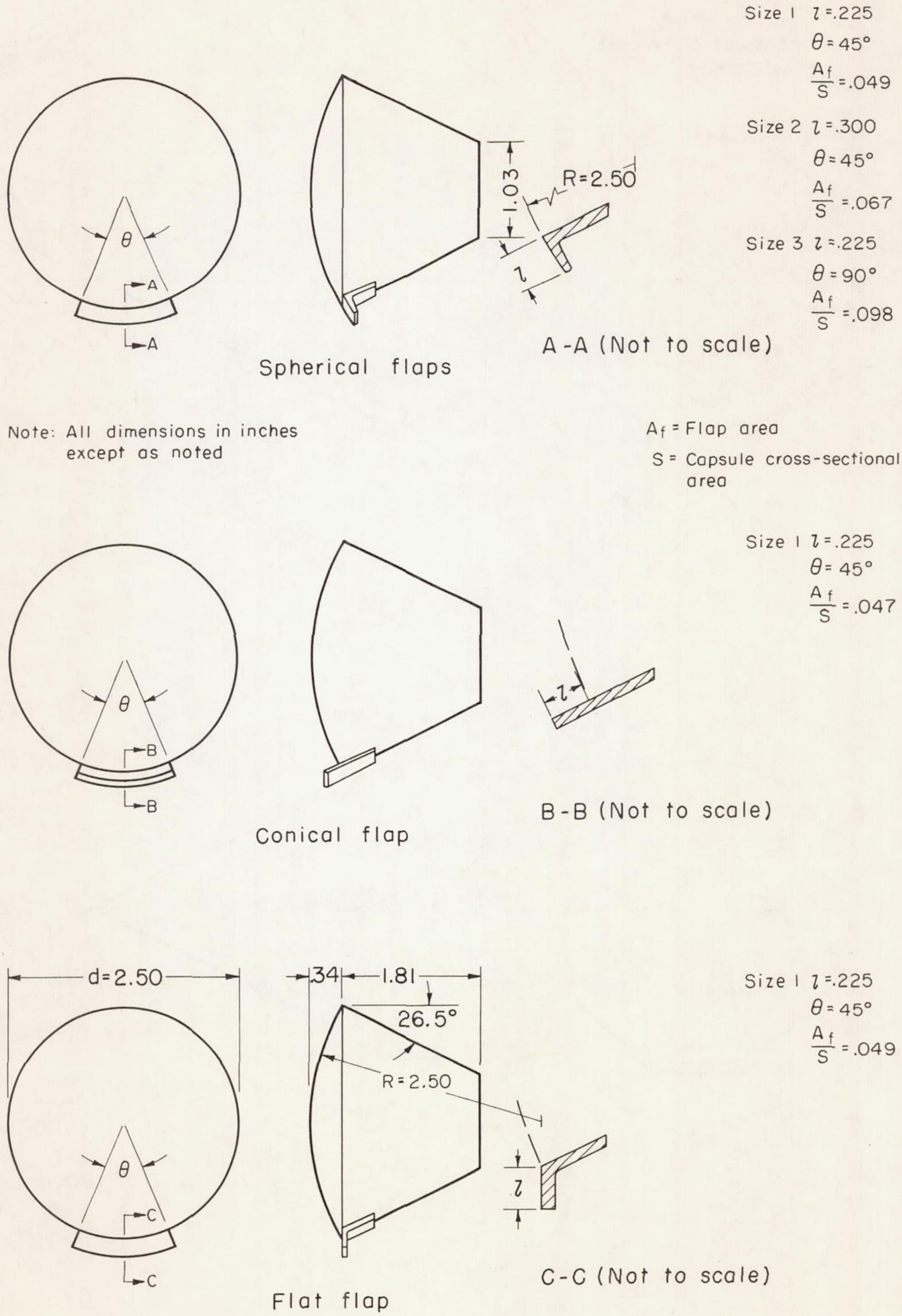

(a) Wind-tunnel models.

Figure 1.- Model arrangement.

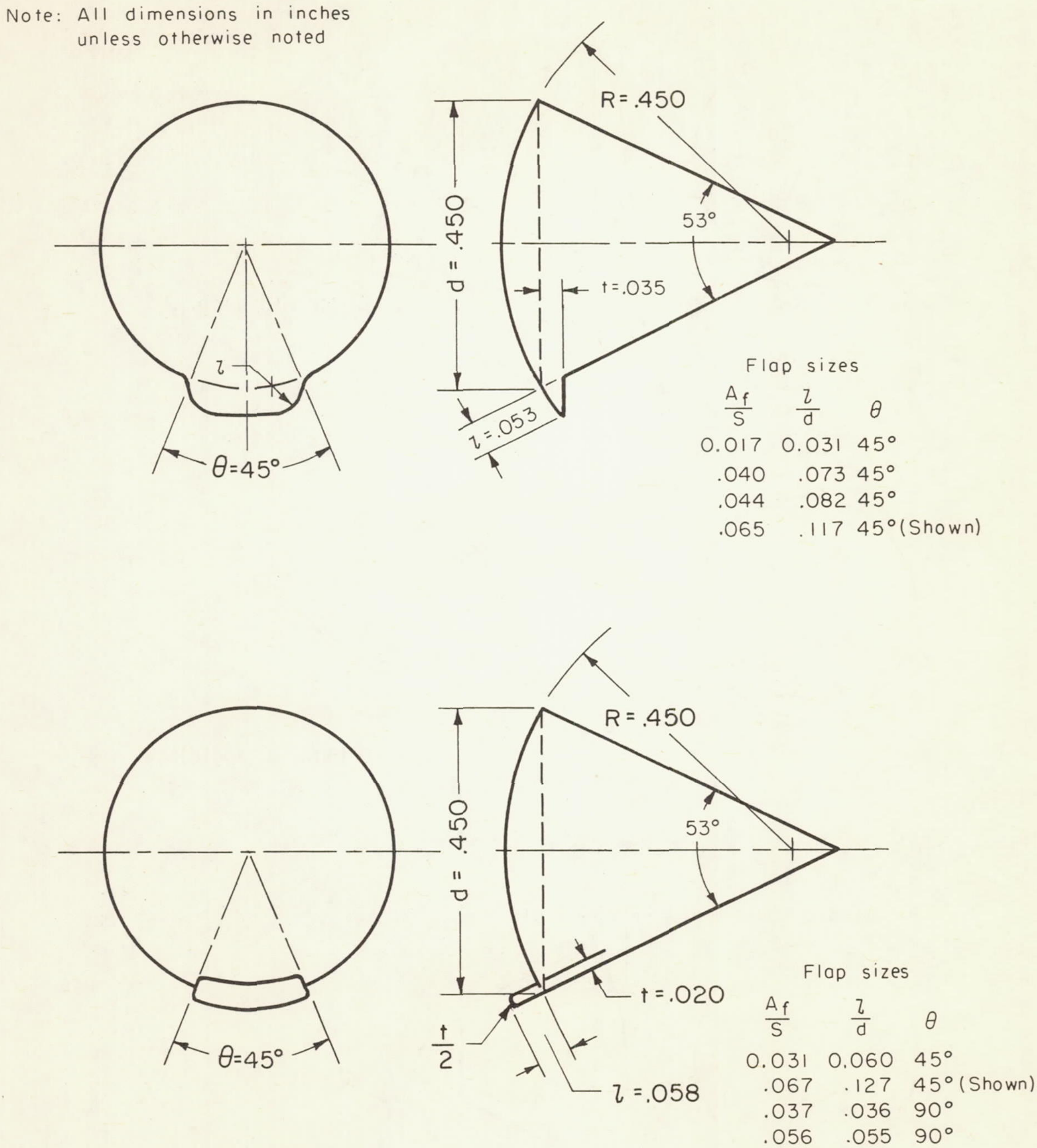

(b) Free-flight models.

Figure 1.- Concluded.

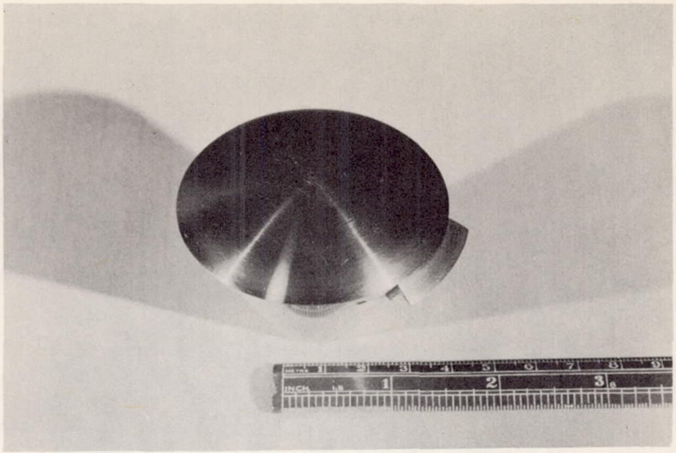

(a) Spherical flap. A-27370

A500

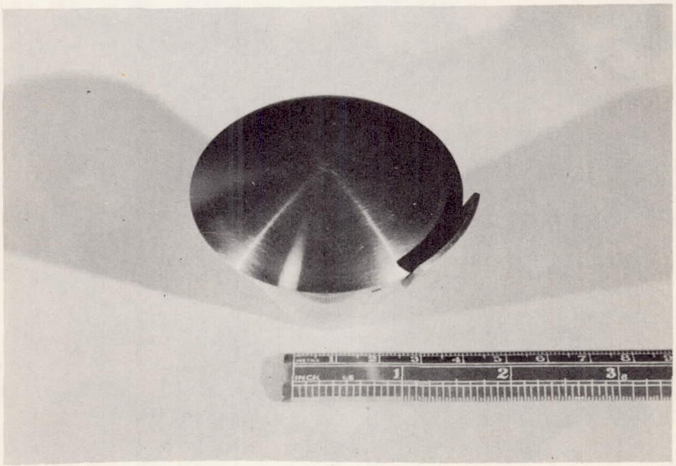

(b) Conical flap. A-27372

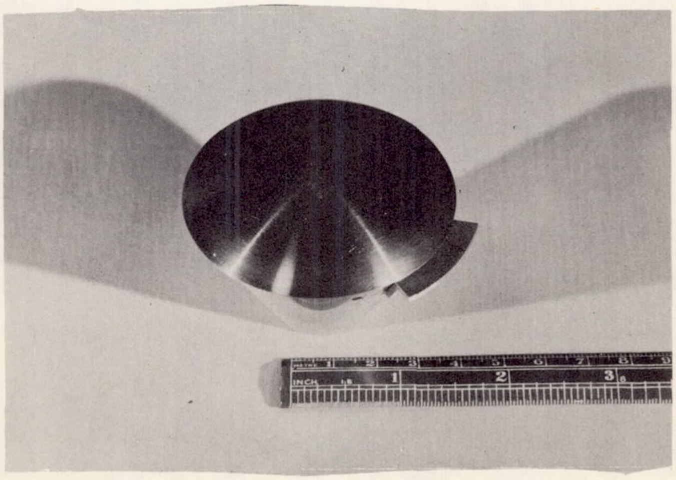

(c) Flat flap. A-27371

Figure 2.- Photographs of wind-tunnel models.

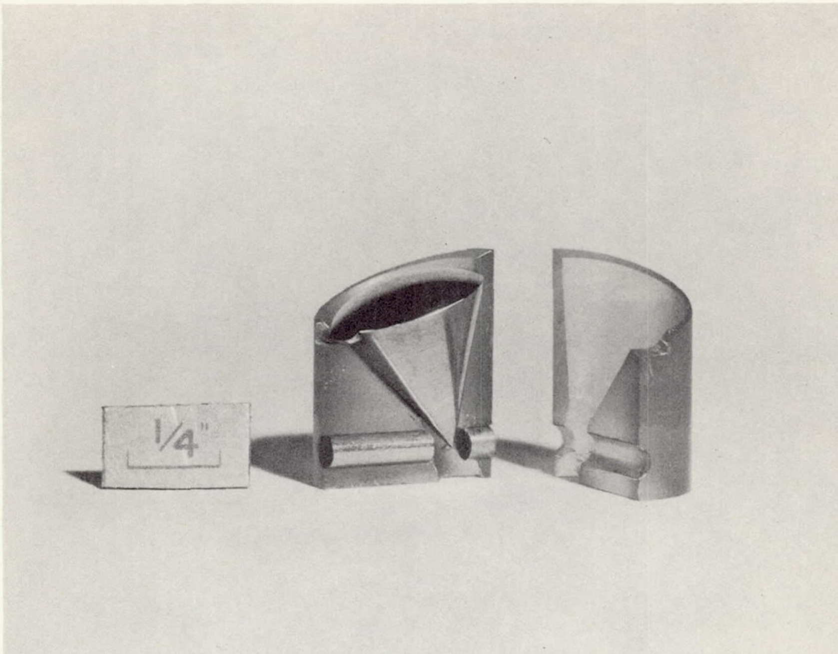

A-28171

(a) Spherical flap.

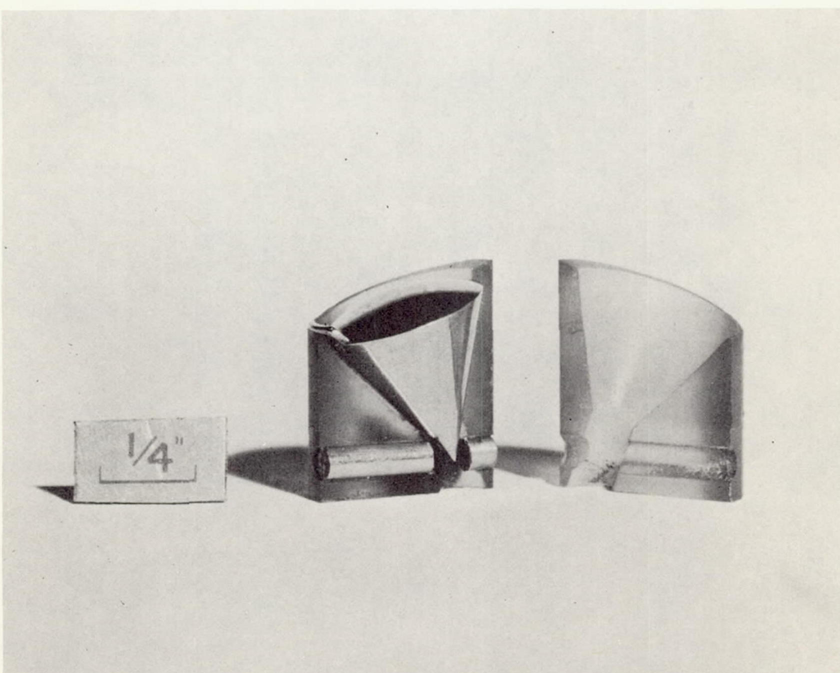

A-28172

(b) Conical flap.

Figure 3.- Photographs of free-flight models and sabots.

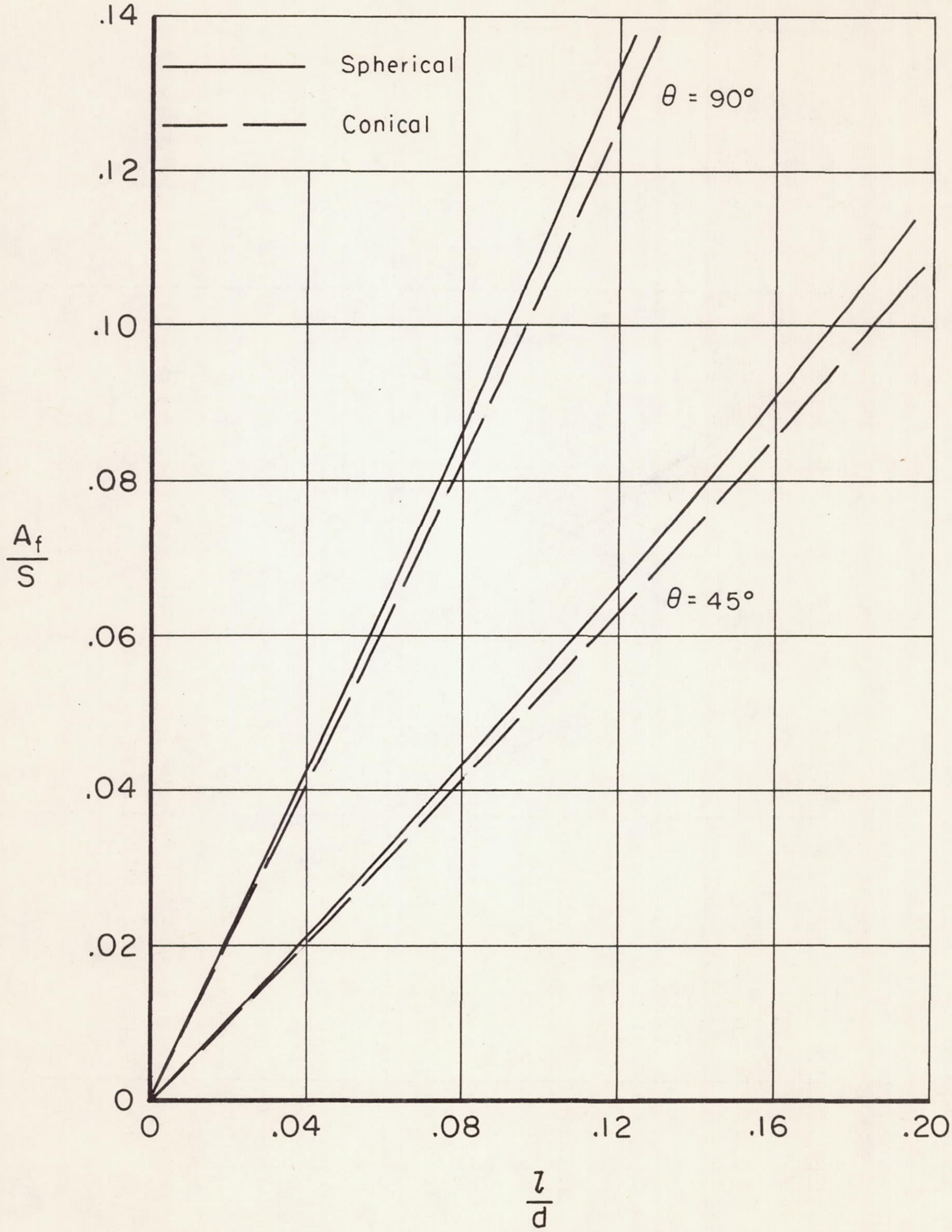

Figure 4.- Variation of flap area with flap extension.

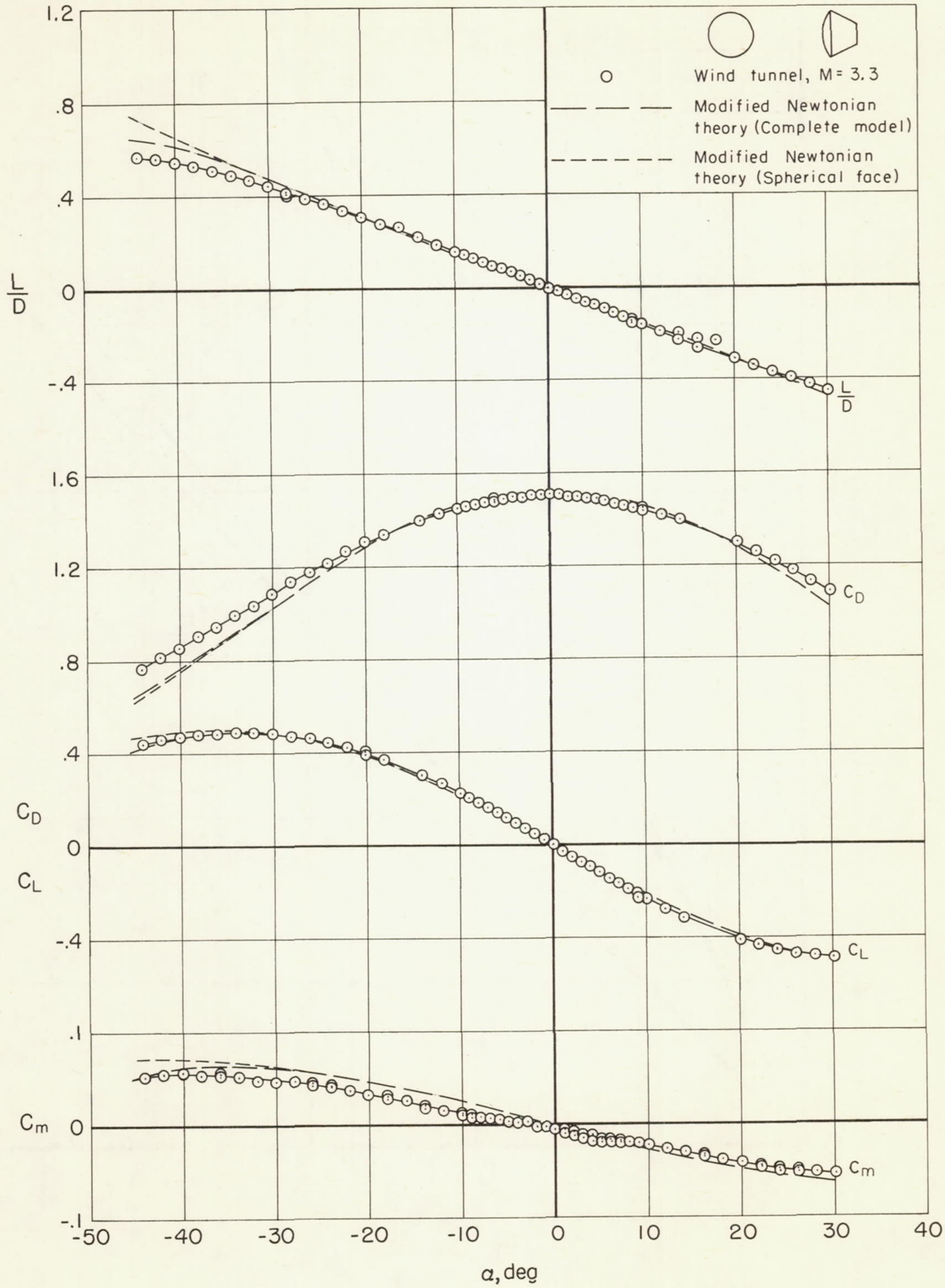

Figure 5.- Aerodynamic characteristics of the basic capsule.

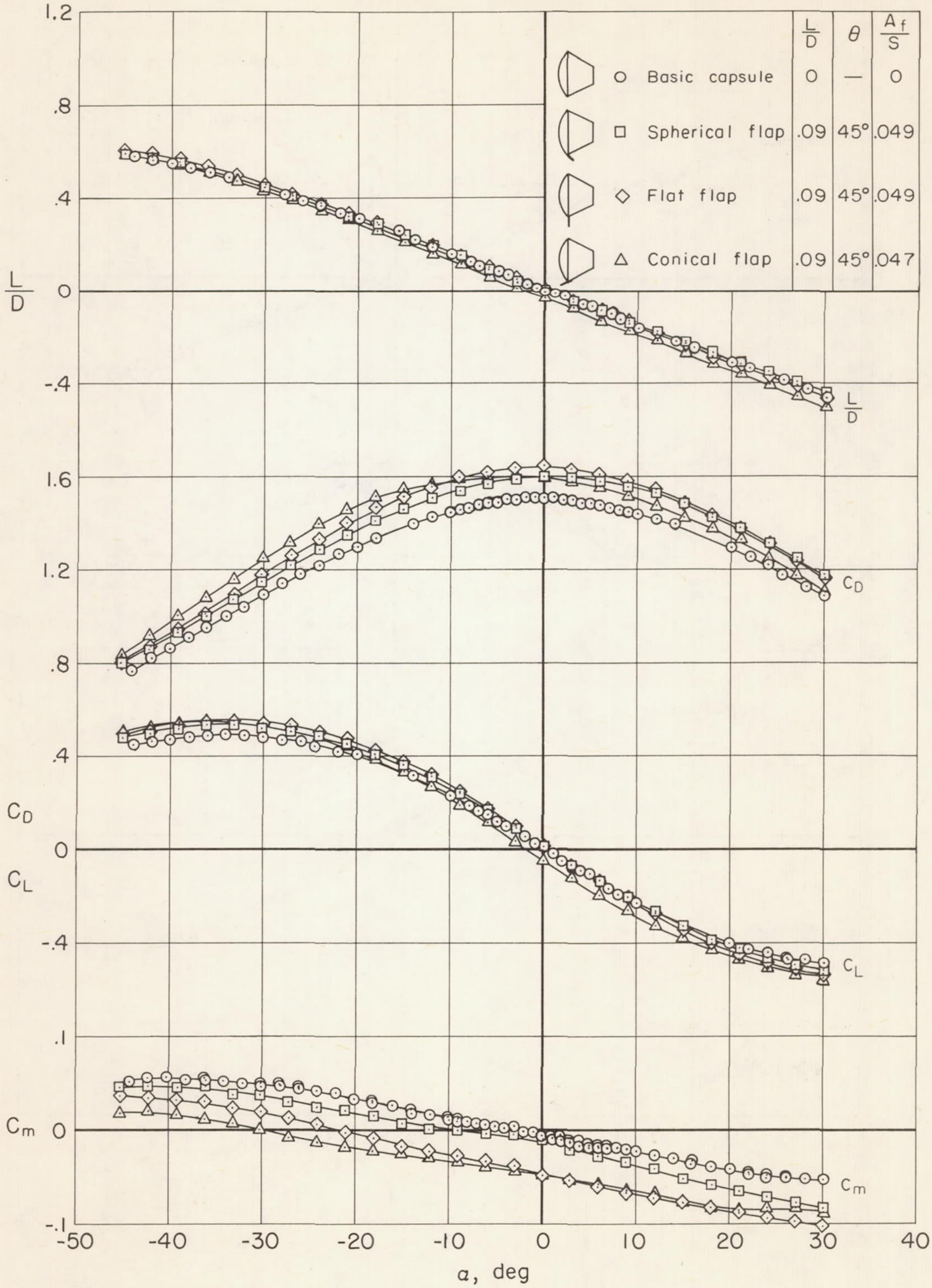

Figure 6.- Effect of flap shape on the aerodynamic characteristics of body-flap combinations.

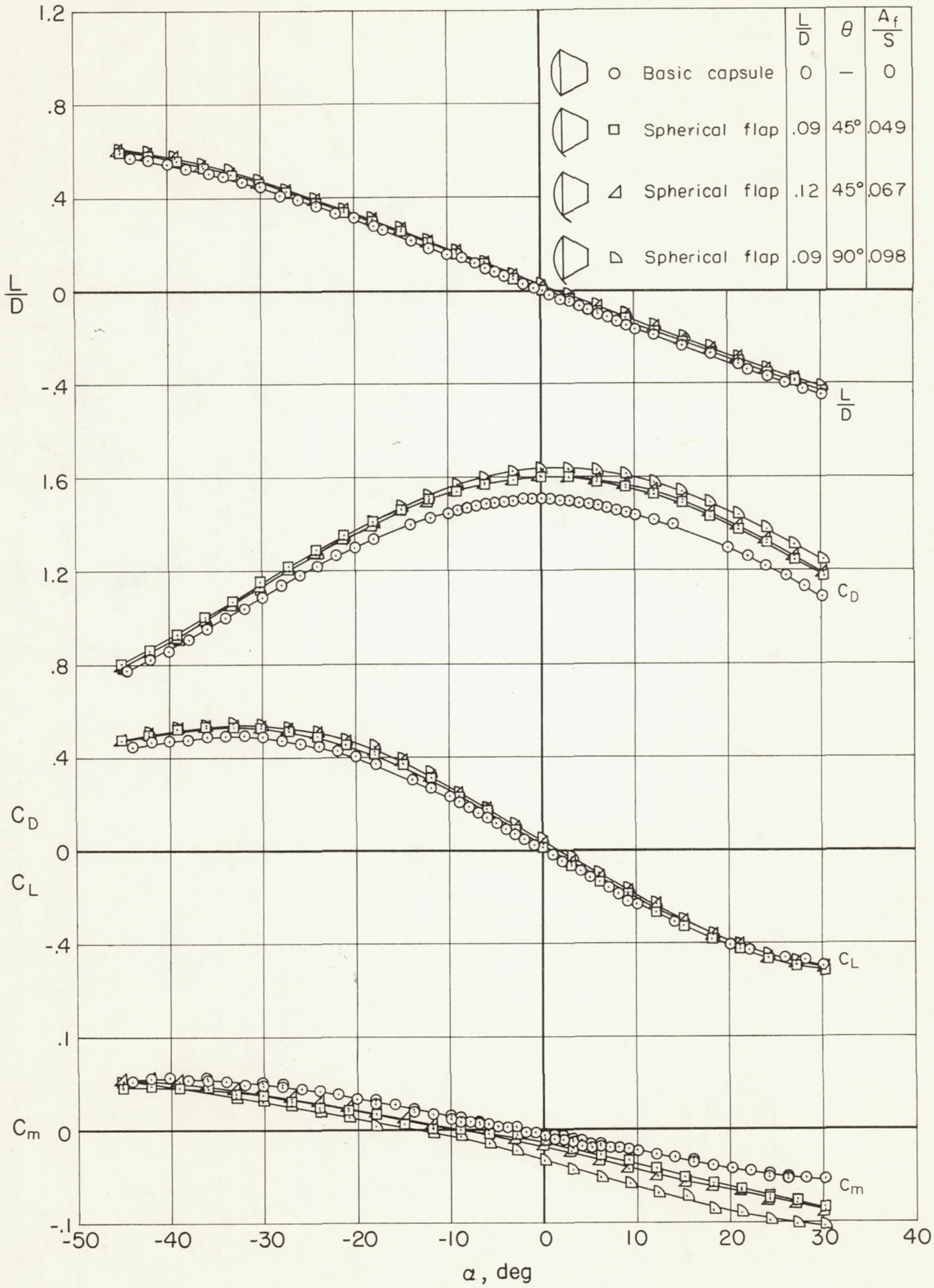

Figure 7.- Effect of flap size on the aerodynamic characteristics of body with a spherical flap.

A
5
0
0

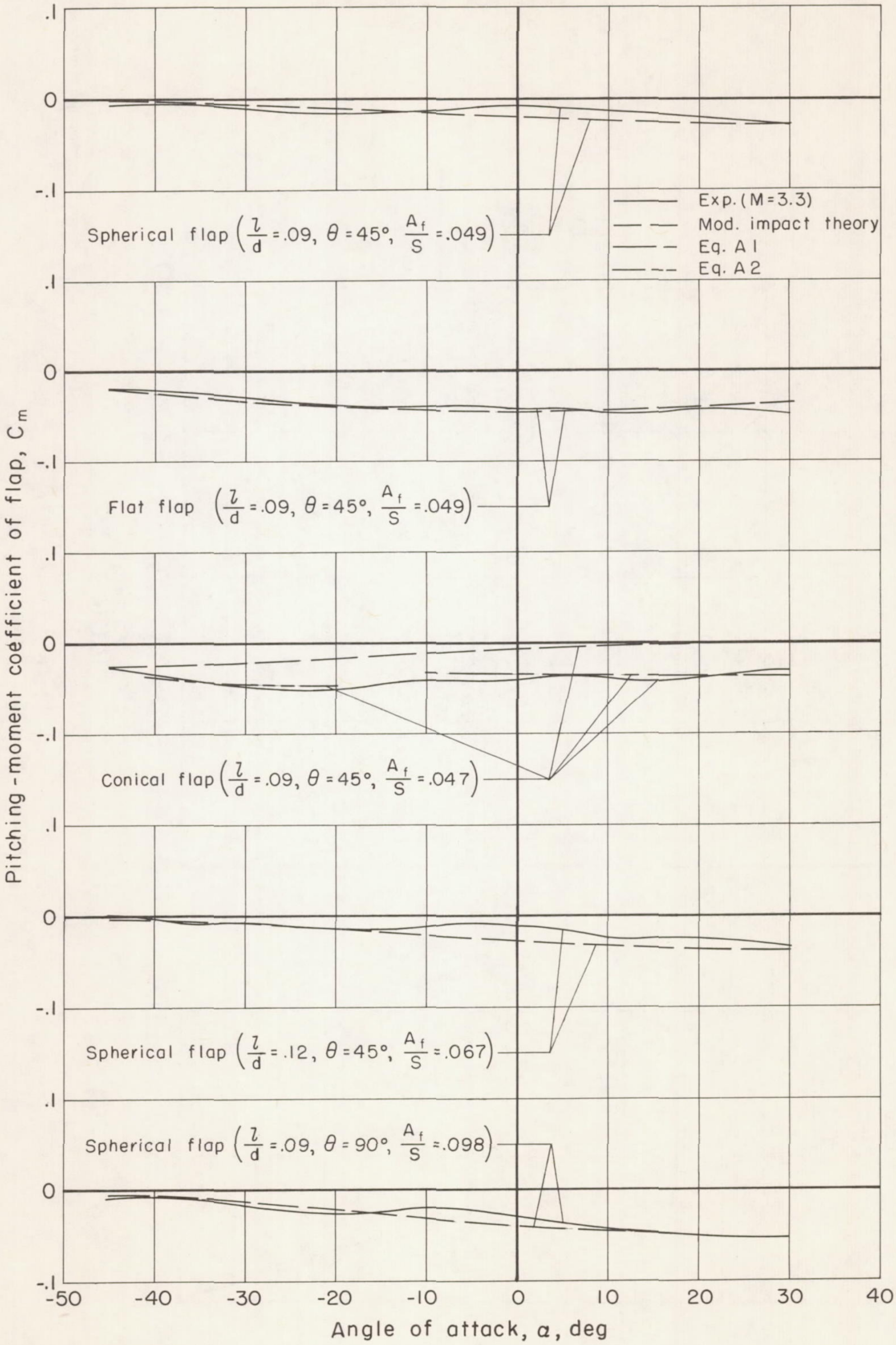

Figure 8.- Pitching-moment coefficients of the flaps.

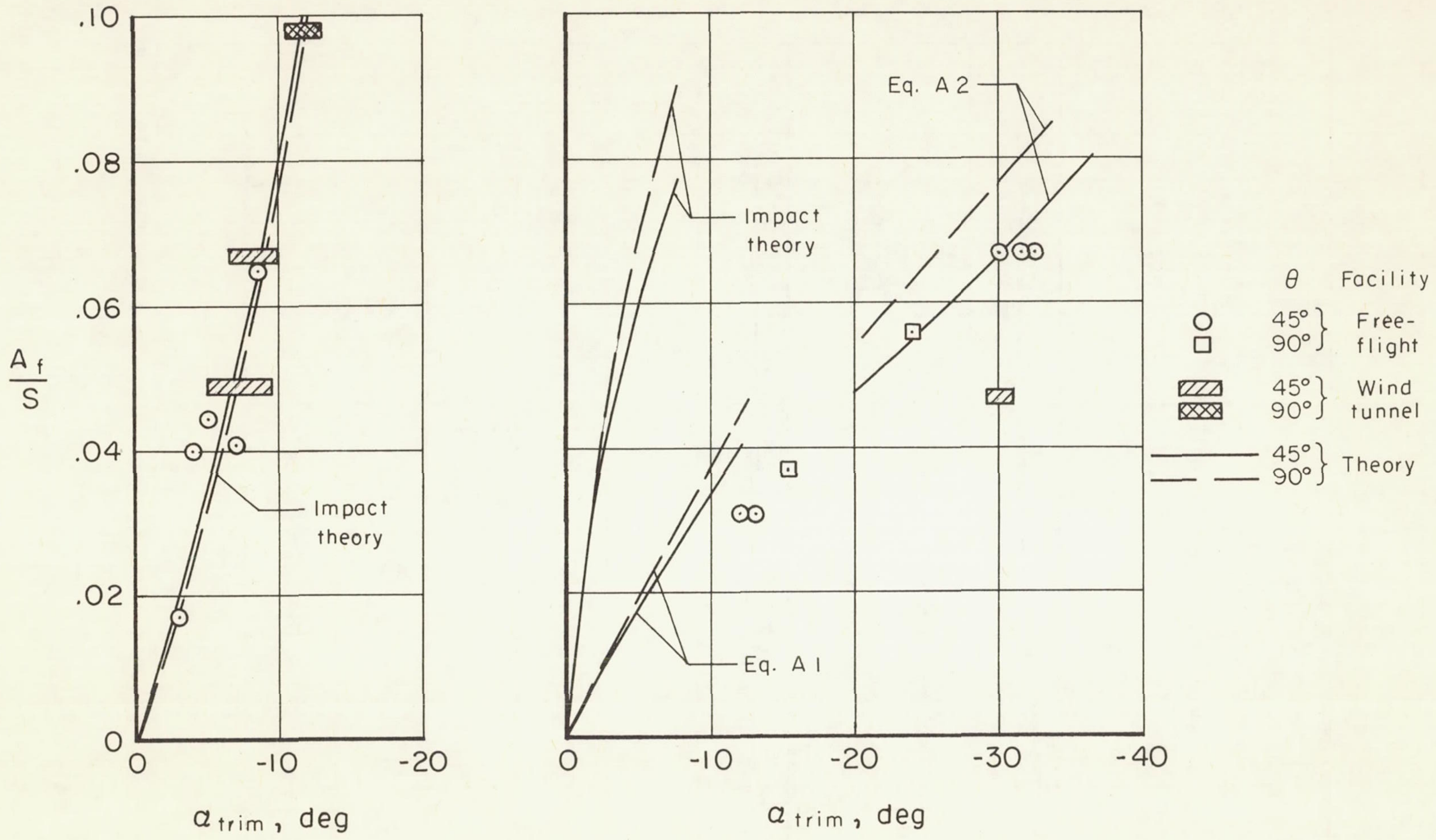

(a) Spherical flap.

(b) Conical flap.

Figure 9.- Trim effectiveness of spherical- and conical-type flaps.

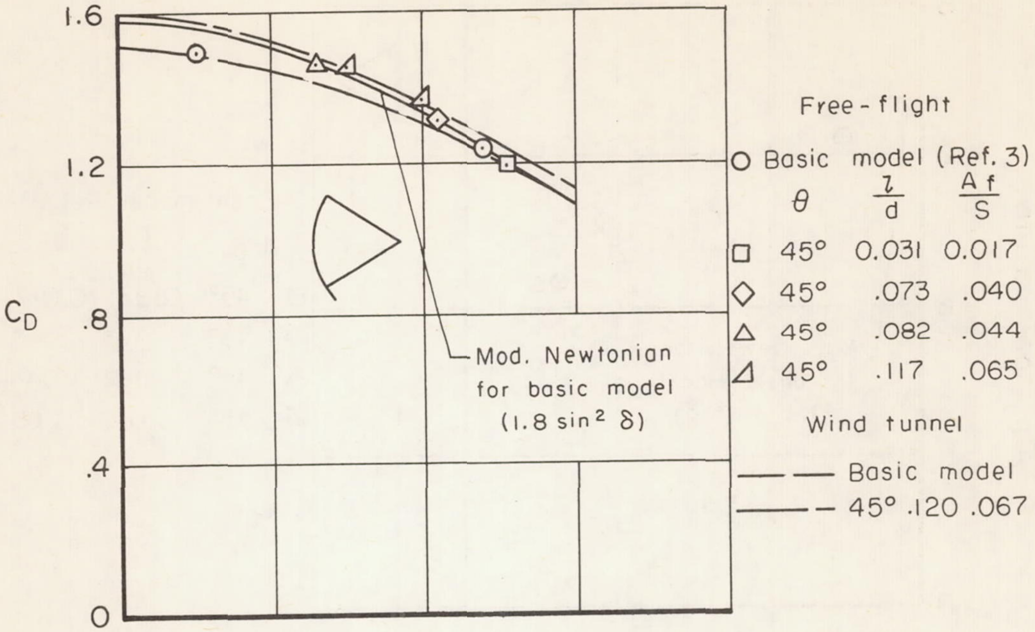

(a) Spherical flap.

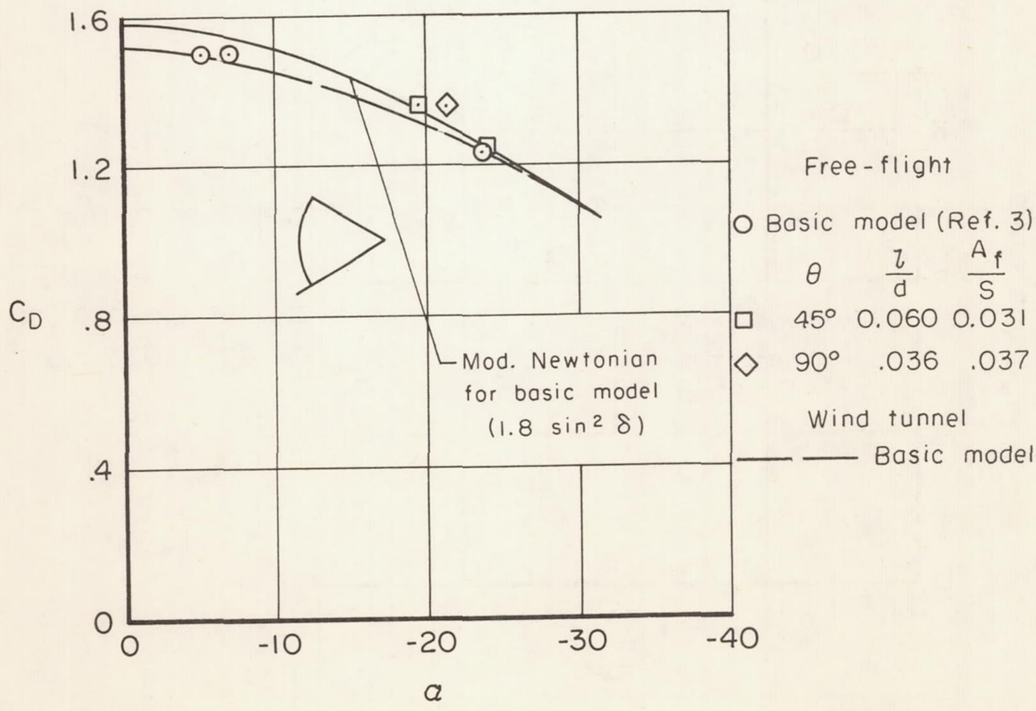

(b) Conical flap.

Figure 10.- Variation of drag coefficient with effective angle of attack.

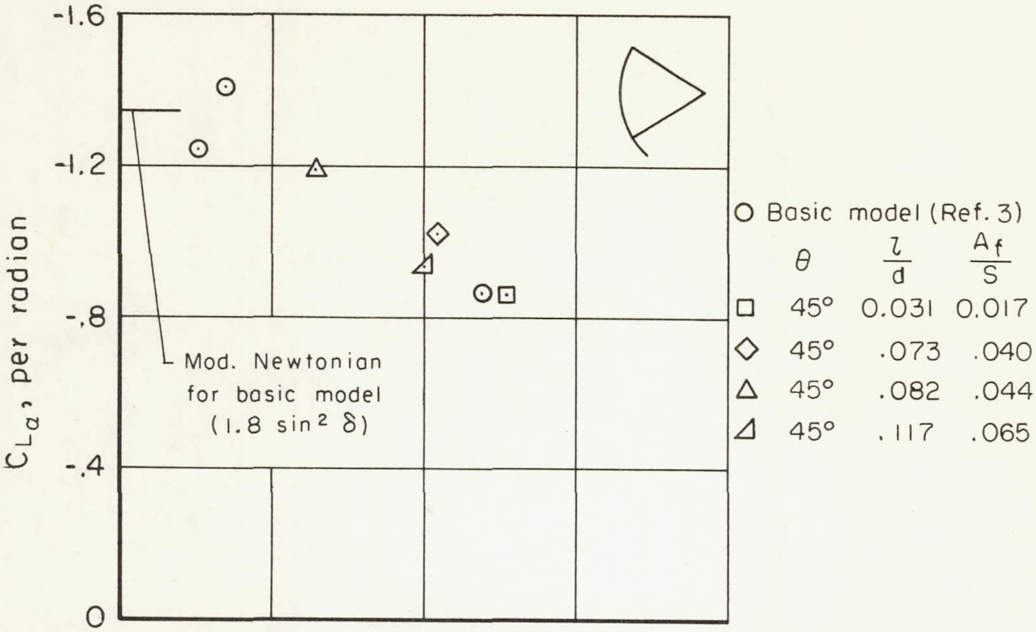

(a) Spherical flap.

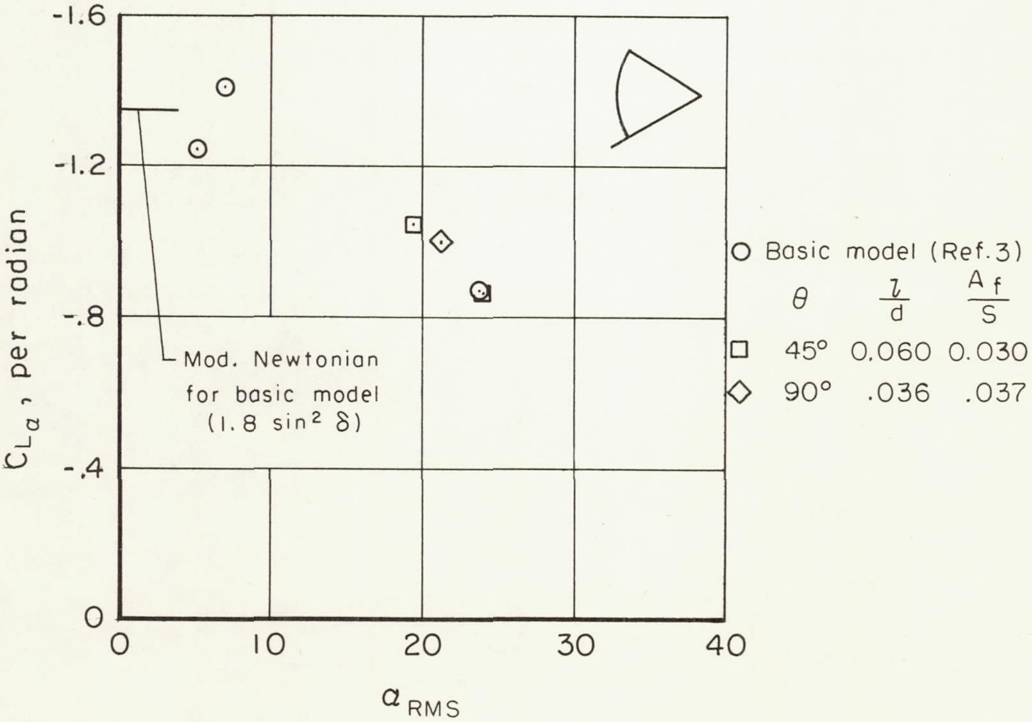

(b) Conical flap.

Figure 11.- Lift-curve slope of free-flight models.

A
5
0
0

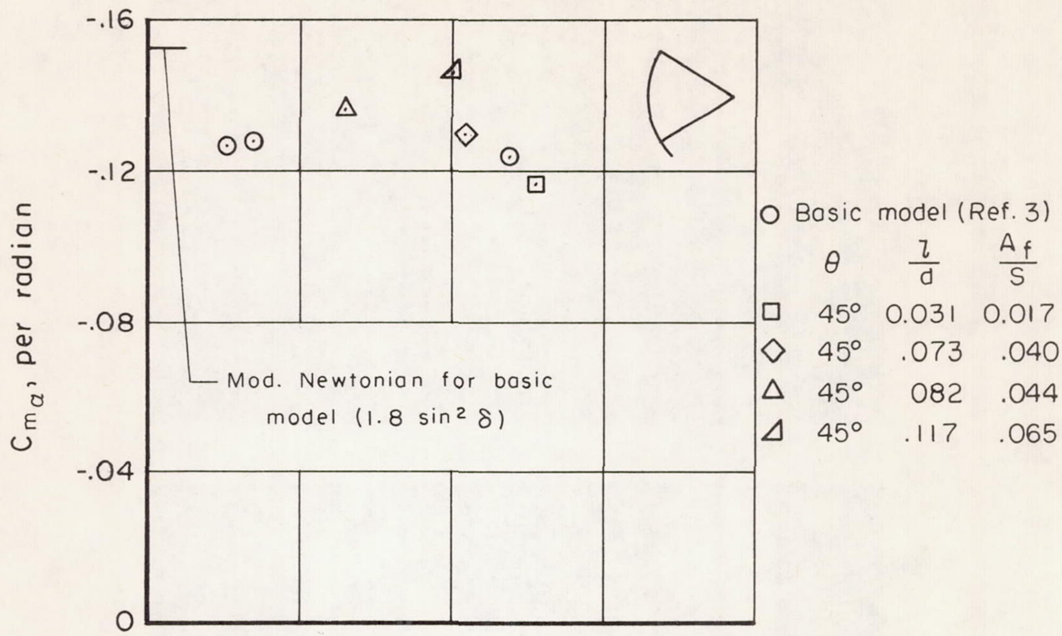

(a) Spherical flap.

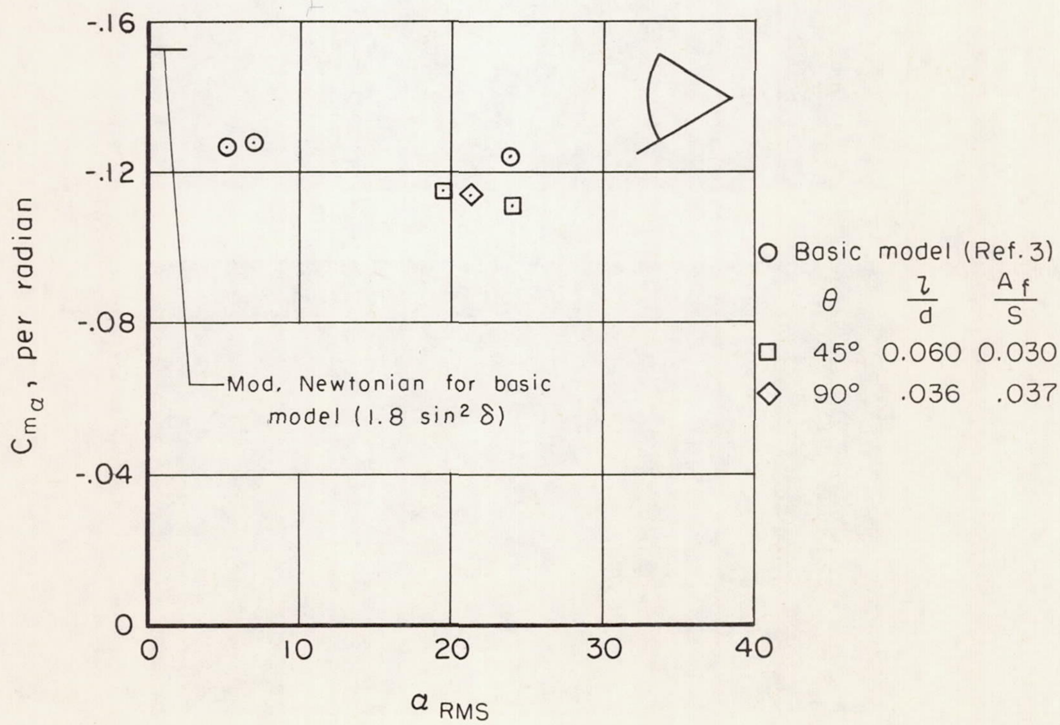

(b) Conical flap.

Figure 12.- Static stability of free-flight models.

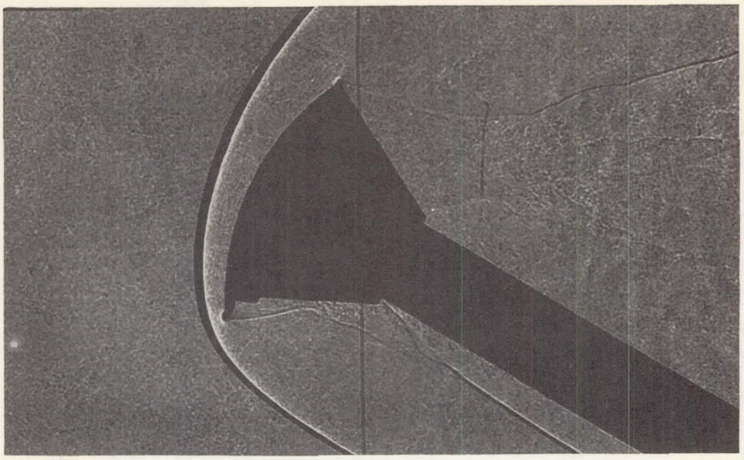

(a) Spherical flap, $\alpha = 30^\circ$.

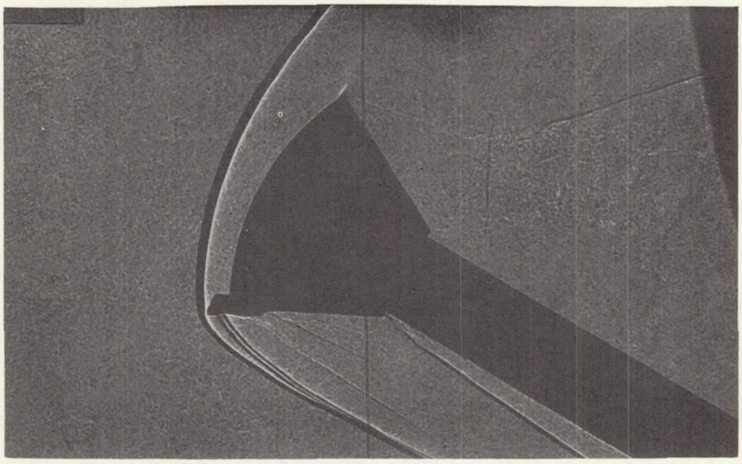

(b) Conical flap, $\alpha = 30^\circ$.

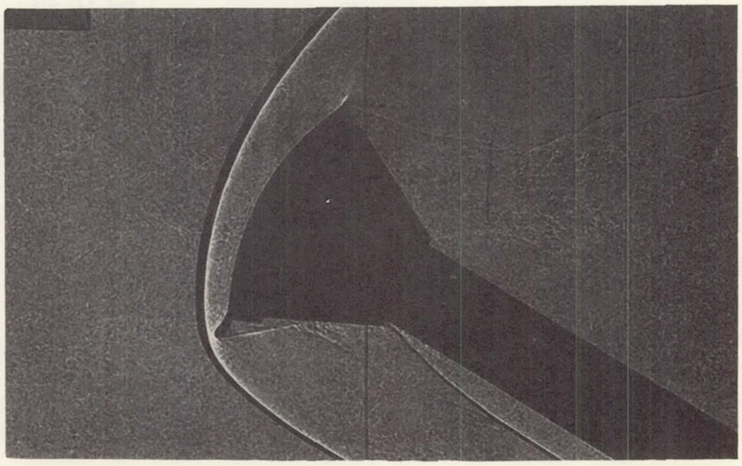

(c) Flat flap, $\alpha = 30^\circ$.

Figure 14.- Typical shadowgraph pictures of sting mounted models in the wind tunnel; $M = 3.3$, $R = 1.25 \times 10^6$.

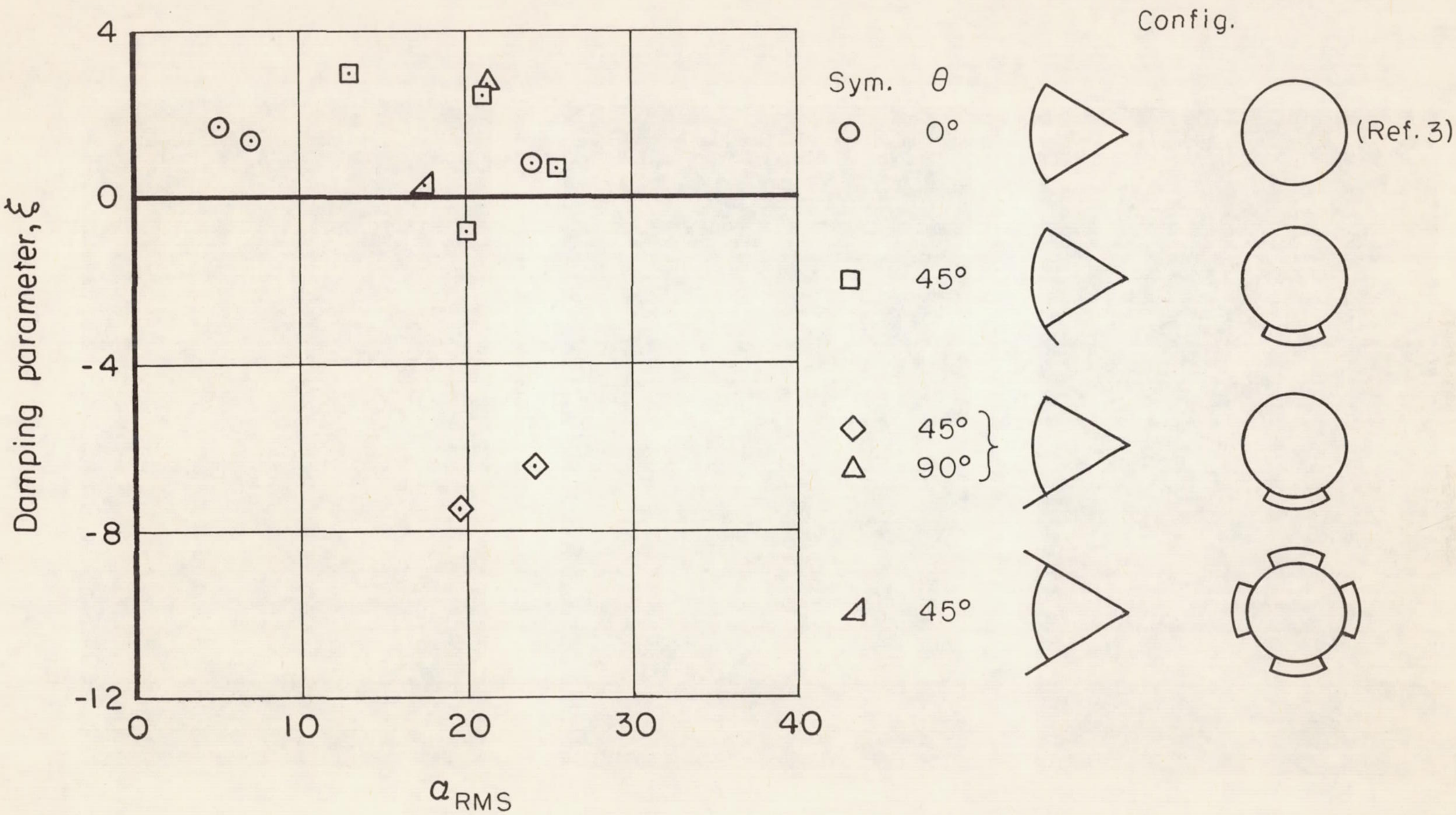

Figure 13.- Dynamic stability of free-flight models.

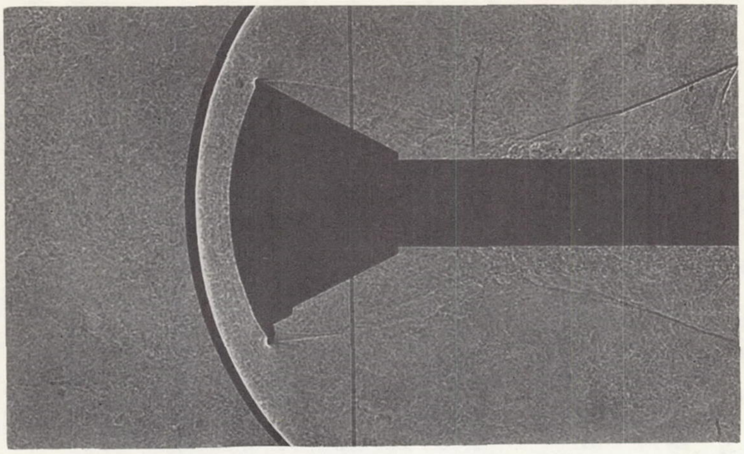

(d) Spherical flap, $\alpha = 0^{\circ}$.

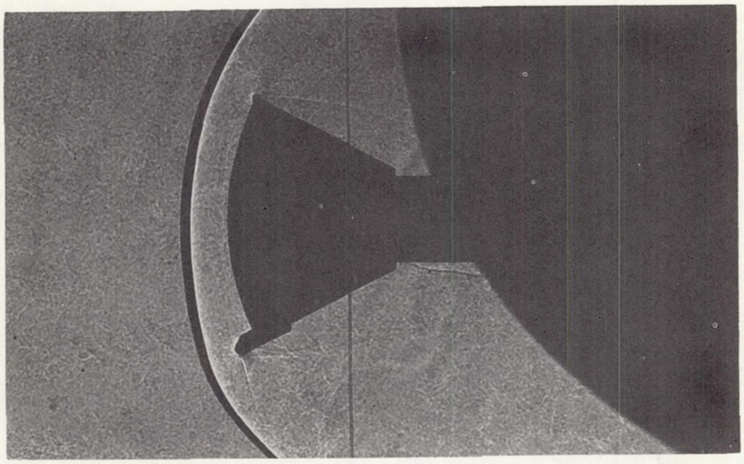

(e) Conical flap, $\alpha = 0^{\circ}$.

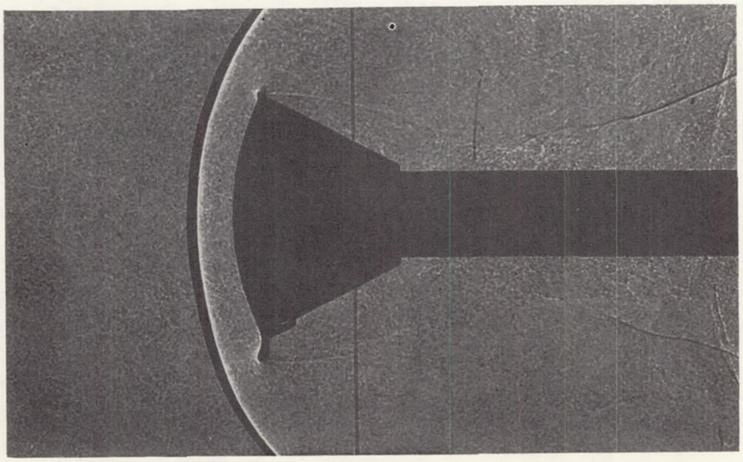

(f) Flat flap, $\alpha = 0^{\circ}$.

Figure 14.- Continued.

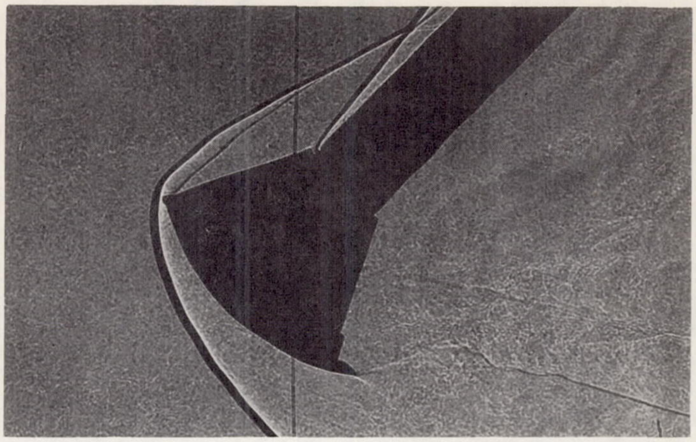

(g) Spherical flap, $\alpha = -45^{\circ}$.

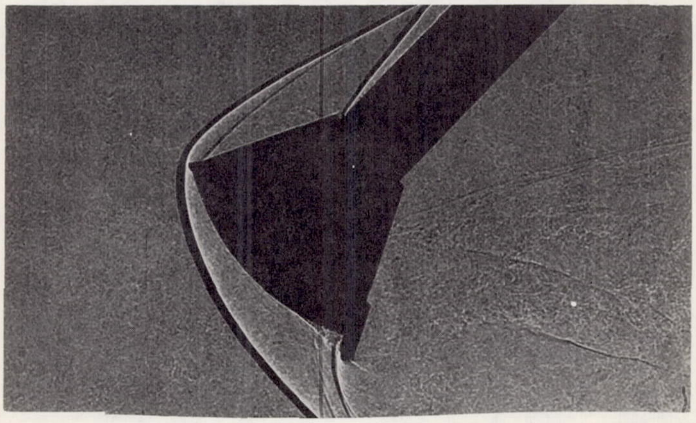

(h) Conical flap, $\alpha = -45^{\circ}$.

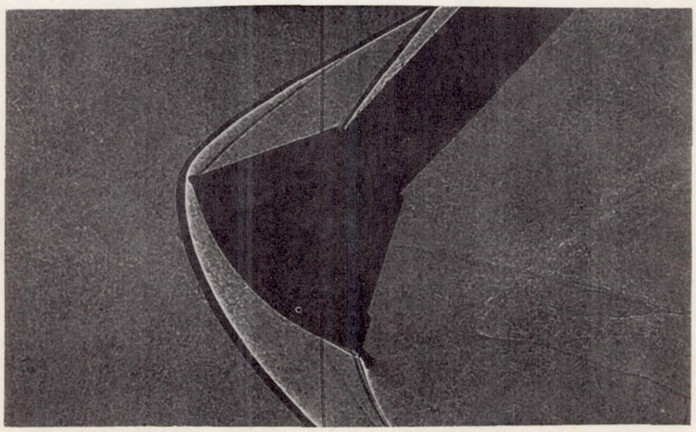

(i) Flat flap, $\alpha = -45^{\circ}$.

Figure 14.- Concluded.

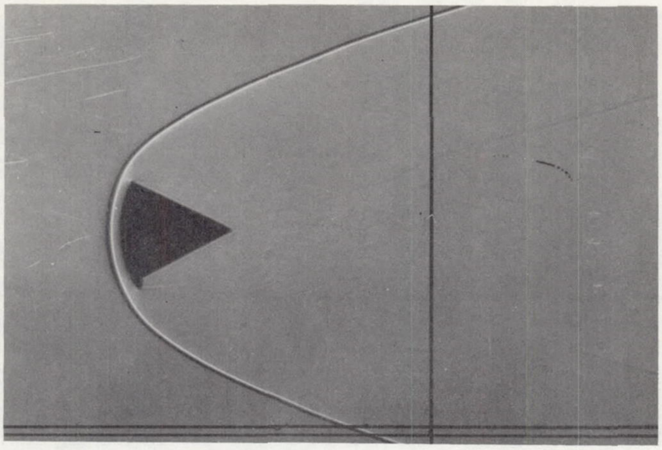

$\alpha = -1.4^{\circ}$

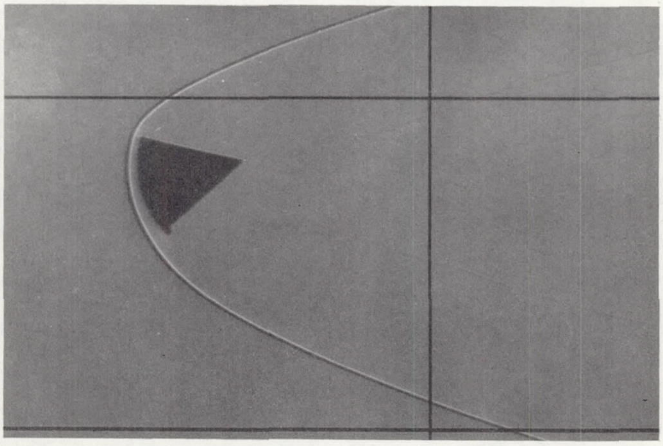

$\alpha = -14.5^{\circ}$

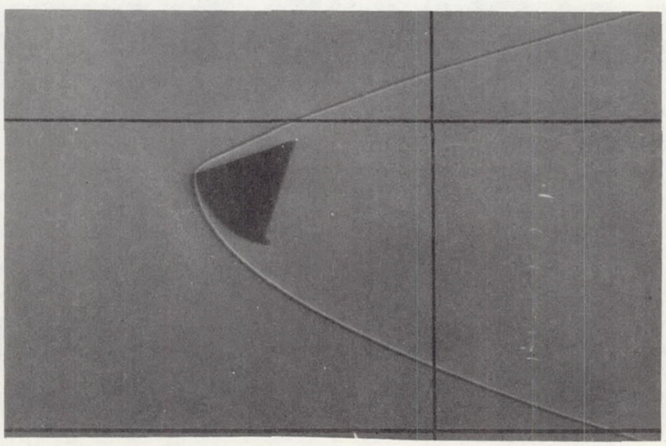

$\alpha = -45.6^{\circ}$

(a) Spherical flap.

Figure 15.- Typical shadowgraph pictures of models in free flight; $M = 5.5$, $R = 0.1 \times 10^{6}$.

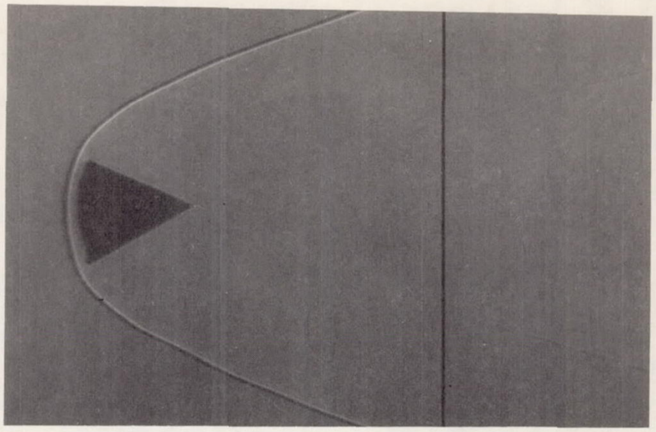

$\alpha = -2.2^{\circ}$

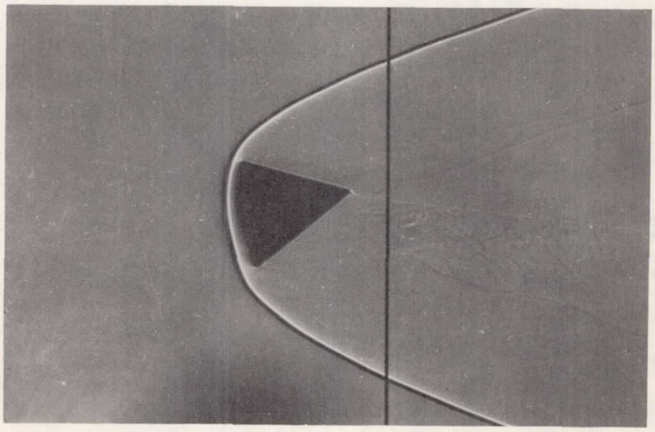

$\alpha = -12.2^{\circ}$

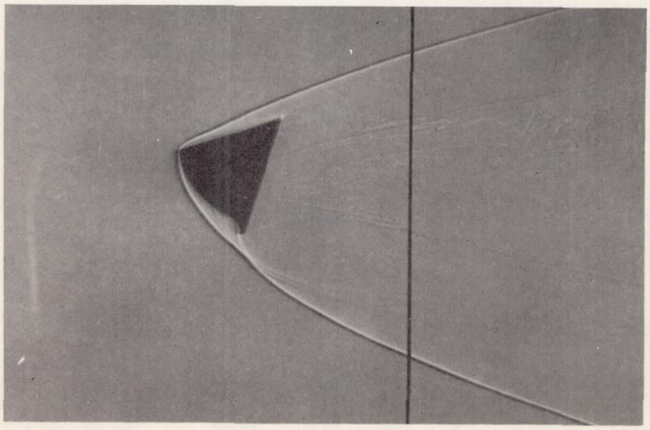

$\alpha = -49.0^{\circ}$

(b) Conical flap.

Figure 15.- Concluded.

CONFIDENTIAL

CONFIDENTIAL